Transient erosion in the Valencia Trough turbidite systems, NW Mediterranean Basin

David Amblas[a], Thomas P. Gerber[b], Miquel Canals[a,*], Lincoln F. Pratson[c], Roger Urgeles[d], Galderic Lastras[a], Antoni M. Calafat[a]

[a]GRC Geociències Marines, Facultat de Geologia, Universitat de Barcelona, E-08028 Barcelona, Spain
[b]Department of Geology, University at Buffalo, NY 14260 Buffalo, USA
[c]Division of Earth & Ocean Sciences, Duke University, NC 27708 Durham, USA
[d]Dept. Geologia Marina, Institut de Ciències del Mar, CSIC, E-08003 Barcelona, Spain

*Corresponding author. Tel: (+34)934021360; Fax: (+34)934021340
E-mail address: miquelcanals@ub.edu (M. Canals)

Keywords: Submarine canyons, turbidity currents, long-profiles, knickpoints, transient erosion

Abstract

Submarine canyons can efficiently drain sediments from continental margins just as river systems do in subaerial catchments. Like in river systems, submarine canyons are often arranged as complex drainage networks that evolve from patterns of erosion and deposition. In the present paper we use a morphometric analysis of submarine canyon-channel long-profiles to study the recent sedimentary history of the Valencia Trough turbidite system (VTTS) in the NW Mediterranean Sea. The VTTS is unique in that it drains sediment from margins with contrasting morphologies through a single “trunk” conduit, the Valencia Channel. The Valencia Channel has been active since the late Miocene, evolving in response to Plio-Quaternary episodes of erosion and deposition. The integrated analysis of long-profiles obtained from high-resolution bathymetric data across the entire turbidite system shows evidence for transient canyon incision in the form of knickpoints and hanging tributaries. Multiple factors appear to have triggered these periods of incision. These include a large debris flow at 11,500 yr BP that disrupted the upper reaches of the VTTS and glacio-eustatic lowstands that forced shifting of sediment input to the VTTS. Based on these inferences, long-term time-averaged incision rates for the Valencia Channel have been estimated. The evidence we present strongly suggests that Foix Canyon has played a key role in the drainage dynamics of the VTTS in the past.

This study builds conceptually on a recent modeling study that provides a morphodynamic explanation for the long-term evolution of submarine canyon thalweg profiles. The procedure and results from this work are of potential application to other submarine sediment drainage systems, past and present, including those containing mid-ocean type valleys like the Valencia Channel.

1. Introduction

Submarine canyons are one of the most intriguing features of Earth's surface. They are some of Earth's largest erosive landforms and the main transport path for sediment accumulating in the deep ocean basins. Not surprisingly, submarine canyons have been a main focus of study for the marine science community. Although submarine canyons were first recognized in the 19th century (Dana, 1863), they were not mapped in detail until the late 20th century following advances in geophysical technology. Today we have submarine canyon images with a resolution comparable to subaerial DEMs, which has allowed us to deepen our understanding of canyon form and evolution.

Though there is still some controversy surrounding submarine canyon genesis (Pratson et al., 2009, and references therein), it is widely accepted that they evolve and grow from the action of sediment gravity flows, mainly turbidity currents (Shepard, 1981), but also other flows like dense shelf water cascades (Canals et al., 2006). The long-term effect of gravity flows passing through a canyon shapes its morphology. Thus canyon morphologic variability is largely due to differences in flow-related factors, such as the characteristic flow size, density and grain size (Pratson et al., 2000; Kneller, 2003; Gerber et al., 2009). Together, these factors and the overall basin setting determine the canyon morphodynamics.

A very useful canyon measure for inferring morphodynamic processes is the along-thalweg depth profile (i.e. canyon long-profile). Like in rivers, the long-profile of canyons tends to display smooth curvature despite the topographic irregularity of the adjacent seafloor. This observation has motivated studies aimed at reconstructing flow properties from canyon and channel long-profiles that are assumed to be in steady-state with an average fluid and sediment discharge (e.g. Pirmez et al., 2000; Kneller, 2003; Pirmez and Imran, 2003; Mitchell, 2005a; Gerber et al., 2009). In addition, submarine canyons show discontinuities in their long profile that resemble widely observed subaerial knickpoints. In river basins, knickpoints are generally interpreted as evidence for downstream base level fall, and their form has been used to infer erosion laws (i.e. detachment- vs. transport-limited erosion) governing upstream migration (Howard et al., 1994; Whipple and Tucker, 2002). Submarine knickpoints have been shown to initiate where tectonic motion displaces the seafloor (e.g. Mitchell, 2006) and where channel levees are breached (e.g. Pirmez et al., 2000). However, there is no consensus on the form of a turbidity-current transport law governing knickpoint migration (Mitchell, 2006; Gerber et al., 2009) or on whether changes in an ultimate submarine "base level" can generate knickpoints (e.g.

Adeogba et al., 2005). Moreover, while subaerial studies of knickpoints have been conducted at the scale of an entire drainage network (Crosby and Whipple, 2006), most submarine examples have been documented over a single reach.

Classically, the sedimentary record of submarine basins has been described using an analysis of depositional bodies, especially outer-shelf prograding clinoforms (e.g. Mitchum et al., 1977; Nittrouer et al., 1986; Cattaneo et al., 2004; Rabineau et al., 2005) and deep-sea fans (e.g. Normark, 1970; Bouma et al., 1986; Palanques et al., 1994; Covault and Romans, 2009). Morphologic anomalies in canyon long-profiles also contain valuable information about previous equilibrium conditions and can be used to unveil the long-term sedimentary history either in single canyons or in submarine valley networks. In the present study we use these anomalies to address the long-term evolution of the entire Valencia Trough turbidite system (VTTS), defined here as the submarine drainage extending from the saddle of the Eivissa Channel, at the southern end of the Valencia Trough, to the Algero-Balearic abyssal plain, at its northern terminus. Our approach is similar to the subaerial drainage basin analysis recently done for the Colorado River (Cook et al., 2009).

Methods for determining terrestrial erosion rates (e.g. cosmogenic radionuclides, fission tracks, He dating) are generally not available in the submarine environment (Mitchell et al., 2003), although recent studies have used optically stimulated luminescence (OSL; e.g. Olley et al., 2004) to date sand grains in modern deep-water transport systems (e.g. Boyd et al., 2008). In this paper we focus on detailed long-profile bathymetry compiled across the large VTTS to roughly estimate maximum time-averaged channel erosion rates. To do this we combine the shape of the network's smooth long-profiles with that of two prominent knickpoints to estimate the depth of entrenchment in the Valencia Channel. We then consider possible triggers for the entrenchment and consequent knickpoint initiation, focusing on processes in both the upper and lower portions of the drainage network. By reconstructing the dynamics of channel adjustment we assess the extent to which turbidite channels adjust their morphology and relief following perturbations to the drainage network.

2. Study Area

The Valencia Channel is the main conduit through which sediment is transported along the deep Catalano-Balearic Basin, i.e. the portion of the Western Mediterranean Basin extending from the Balearic Archipelago to the southeast with the Iberian mainland as its northwestern limit (Palanques and Maldonado, 1985; Alonso et al., 1991; Canals et al., 2000; Amblas et al., 2006). This deep-sea channel (Fig. 1), classified by Canals et al. (2000) as a mid-ocean type valley, routes sediment from a network of submarine canyons and canyon-valley systems crossing the Ebro and Catalan margins, and also from localized large unconfined landslides (Alonso et al., 1991; Canals et al., 2000, Lastras et al., 2002; Amblas et al., 2006). The 430 km long Valencia Channel starts approximately at 1600 m water depth and terminates on the Valencia Fan (Palanques and Maldonado, 1985), which lies on the northernmost part of the Algero-Balearic abyssal plain at about 2800 m water depth (Fig. 1).

Almost the entire length of the Valencia Channel follows the Valencia Trough axis, and thus parallels the bordering Iberian and Balearic continental margins. The Valencia Trough is one of the extensional sub-basins that define the northwestern Neogene Mediterranean rift system (Maillard and Mauffret, 1999). The trough, Late Oligocene–Early Miocene in age, is delineated by NE–SW oriented horsts and grabens (Roca et al., 1999).

Incision in the Valencia Trough may have originated under subaerial conditions during the Messinian salinity crisis (Cita et al., 1978; Alonso et al., 1995; Maillard et al., 2006). Some of the submarine valleys draining into the Valencia Channel are also of Messinian origin, though there is not a one to one relationship between Messinian Canyons and present-day Canyons (e.g. Urgeles et al., 2010). Other canyons appear to have formed during Plio-Quaternary lowstands and some appear to coincide with tectonic faults (Alonso et al., 1991, 1995; Berné et al., 1999; Amblas et al., 2004, 2006; Kertznus and Kneller, 2009; Petter et al., 2010). However, the current shape of the VTTS reflects submarine erosion and deposition by sediment gravity flows during Pliocene and Quaternary times (Palanques et al., 1994; Alonso et al., 1995).

Following the margin morphologic analysis performed by Amblas et al. (2006), we define the Valencia Channel upper course as the Ebro Margin reach, the middle course as the South Catalan Margin reach, and the lower course as the segment downstream from Blanes Canyon junction, marking the boundary with the North Catalan margin (Figs. 1 and 2). This classification slightly differs geographically to that proposed by Alonso et al. (1995) before comprehensive multibeam bathymetry data from the area were available. The Valencia Channel is unique in that it incorporates sediment output from two distinctly different sediment routing systems in a semi-confined basin. The upper course of the

Valencia Channel is fed by numerous, relatively small canyon-channel systems (i.e. the Ebro turbidite system) initiating on the outermost section of the wide Ebro constructional shelf (60–80 km) or on the upper slope (Canals et al., 2000; Kertznus and Kneller, 2009). On the other hand, the middle course is fed by a few large canyons incised into the rather narrow South Catalan shelf and in a smooth slope, with evidence for significant sediment bypassing to the Valencia Channel (Amblas et al., 2006). This contrast between neighbouring margins has motivated the development of a morphodynamic model describing the controls on the long-profile shape of submarine canyons (Gerber et al., 2009).

3. Submarine canyon-channel morphology

During the last decade several cruises performed extensive multibeam surveying in the Catalano-Balearic Basin, which provided an almost complete image of the VTTS. Survey and data set characteristics are thoroughly described in Amblas et al. (2006). The data resolution (50 m) allows us to characterize not only the largest sediment conduits (i.e. submarine canyons and canyon-channel systems) in the basin but also details of their morphology, including thalwegs, axial incisions, canyon walls, levees and terraces.

As the major focus of our study, we extracted the long-profiles of major canyons feeding the Valencia Channel by tracing thalwegs on the bathymetry. The modern VTTS is bound by Orpesa Canyon (the southernmost modern tributary of the Valencia Channel) and Blanes Canyon (the northernmost modern tributary of the Valencia Channel) (Fig. 1). These long-profile elevation-distance plots are shown together with the Valencia Channel profile in Fig. 2a, which illustrates the entire VTTS up to its distal end (i.e. Valencia Fan). In general, long-profile curvature is upward concave (i.e. decreasing in downslope direction), though there are slight differences between them.

Blanes Canyon (length: 184 km; sinuosity: 1.47) is the northernmost of the Valencia Channel tributaries and is incised up to 1500 m into the Catalan margin continental shelf. The canyon head parallels the nearby (less than 4 km) coastline and the upper course is characterized by steep (more than 25º) gullied walls (Lastras et al., 2011). The structural grain beneath the base of the slope may be responsible for the meandering morphology of the lower course flat-floored channel (Amblas et al., 2006). Blanes Canyon joins the lower Valencia Channel segment at approximately 2600 m water depth (Fig. 3f). The Arenys (length: 76 km; sinuosity 1.06) and Besòs (length: 79 km; sinuosity: 1.03) canyons are mostly restricted to the slope and rise and display a linear NW–SE trend. Both canyons are incised up to 470 m into the Catalan margin slope. Canyon-walls have few gullies and the thalwegs are almost flat-floored with nearly constant width. Arenys and Besòs canyons converge immediately above the Valencia Channel and join it as a wide single valley in 2380 m of water depth (Fig. 3e). Foix Canyon (97 km long) is located south of the Llobregat Delta and is the southernmost of the Catalan Margin canyons. Its upper course consists of two similar highly sinuous arms that merge at 1430 m depth. The southern arm hangs 220 m above the northern one, indicating more recent activity of the latter. Total sinuosity of the canyon calculated from its northern arm is 1.23, which is probably influenced by tectonic faults beneath its upper course (Amblas et al., 2006). Maximum canyon wall gradients (up to 23º) and down-cutting (up to 480 m) are observed in the upper course. The lower course of Foix Canyon becomes wider and flat floored and joins the Valencia Channel at 2180 m water depth (Fig. 3d). Vinaròs (length: 78 km; sinuosity: 1.24), Hirta (length: 74 km; sinuosity: 1.24) and Orpesa (length: 68 km; sinuosity: 1.10) canyons are the only Ebro margin tributaries to the Valencia Channel. These canyons, also called respectively “5”, “4” and “3” in Canals et al. (2000), display narrower thalwegs and better-developed constructional levees than those in the Catalan margin. They join the Valencia Channel at 2030, 1900 and 1775 m water depth respectively (Fig. 3a–c). The Columbretes Grande Canyon, called “1” in Canals et al. (2000), is located south of the Ebro margin and it is disconnected from the VTTS (Fig. 1). This 75 km long canyon shows the highest sinuosity (1.40) of the studied margin and it develops atop a convex relief along the continental slope and rise, ending into the deep basin approximately at 1350 m water depth.

The Valencia Channel shows maximum incision (370 m) in the middle course, about 150 km away from the head, downstream from Foix Canyon junction (Fig. 2c and 4). In this segment the deep-sea channel achieves high sinuosity (Fig. 1) and maximum channel-wall steepness (up to 18º). The Valencia Channel thalweg shows a very gentle slope (maximum: 0.6º) with an upward concave curvature along most of its length (Fig. 2b). Large terraces have been identified along the Valencia main course, two along the Ebro margin-reach and six along the South and North Catalan margin reach of the Channel (named T1–T8 in Fig. 3). Sidescan sonographs obtained using the 30 kHz TOBI system show numerous instability features in the Valencia Channel flanks near the Vinaròs junction (Fig. 5).

For the purpose of comparing distance-relief plots for each canyon feeding the Valencia Channel, best-fit surfaces to intercanyon margin profiles are computed. These are obtained by interpolating a surface from bathymetric control points on canyon and channel interfluves. The surface reveals a hypothetical smooth margin that provides a reference elevation for calculating canyon relief along the trace of the canyon thalwegs. Distance-relief plots normalized by the total relief show outstanding differences in the amount of canyon entrenchment (Fig. 6). Southern canyons (Hirta, Vinaròs and Orpesa Canyons) display lower relief than northern canyons (Blanes, Besòs and Foix canyons) and have lower courses that are mostly perched above the surrounding basin floor (negative relief) showing predominance of depositional processes along the lower course of channels in the Ebro Margin.

Most of the Ebro and Catalan canyon-channel tributaries grade smoothly into the Valencia Channel (i.e. no jump in the long profile elevation), but on closer inspection anomalies are seen at or near some junctions (Figs. 3, 5 and 7). Hirta Canyon appears to be hanging 60 m above the Valencia Channel, and Vinaròs Canyon shows a sharp increase in slope at a long-profile discontinuity 8 km upstream of its junction. We describe these features as knickpoints and discuss their morphodynamic implications in the following section.

4. Discussion

4.1. Long-profile analysis

The concordance between the Valencia Channel and most of its tributaries (Blanes, Besòs, Arenys, Foix and Orpesa, Fig. 3) suggests tandem entrenchment of the submarine drainage network. As pointed out by Mitchell (2005b), this is essentially an application of Playfair's Law for fluvial systems (Playfair, 1802; Niemann et al., 2001) to submarine channel networks. This implies that turbidity currents occur frequently enough to keep each tributary confluence at the same elevation as the Valencia Channel. This is clearly not the case for the prominent knickpoints seen on the long-profiles of Vinaròs and Hirta canyons (Fig. 3).

The knickpoint in Vinaròs Canyon (Fig. 5) indicates localized erosion across the steepened step that defines it. We assume that the disequilibrium steepening was caused by a change in the Valencia Channel's entrenchment relative to Vinaròs Canyon, since no hard variations in substrate erodibility has been documented in the area (Field and Gardner, 1990; Alonso et al., 1990, 1995; Canals et al., 1995). In this view, the long-profile below the knickpoint is in equilibrium with the current Valencia Channel but the upstream segment defines a long-profile that is continuous with that of a relict Valencia Channel thalweg. In other words, the location of the knickpoint marks the boundary between the adjusted and unadjusted reaches of the canyon-channel system, and has migrated upstream from its junction with the Valencia Channel while maintaining its steep form (Figs. 5 and 7).

We interpret Hirta Canyon's hanging terminus similarly. Yet unlike Vinaròs Canyon, Hirta Canyon's knickpoint is evidently stationary. We therefore infer that turbidity-current activity has largely shutdown in Hirta Canyon, freezing the knickpoint as a hanging valley (Figs. 3b and 7).

We illustrate the geometry of the long-profile adjustment using simple least-squares fits to the Ebro margin long-profiles. We choose a power-law slope-distance relation for each canyon following process-based studies on canyon form (Mitchell, 2004; Gerber et al., 2009). We first fit the concordant long-profiles of the Orpesa Canyon and the Valencia Channel (profiles 1 and 2, Fig. 7). We then fit the segments of Hirta and Vinaròs canyons that lie above the observed knickpoints and extend the fitted profiles along the course of the Valencia Channel (profiles 3 and 4, Fig. 7). We interpret the basinward projection of the Hirta and Vinaròs long-profile fits as an estimate for a relict Valencia Channel long-profile. The average depth difference between the extrapolated profiles and the modern Valencia long-profile in the present junction is 140 m for the Vinaròs Canyon and 60 m for the Hirta Canyon. Both extrapolated profiles approximate the elevation of numerous terraces observed above the modern Valencia thalweg (Figs. 3 and 7).

The long-profile fits in Fig. 7 imply that entrenchment of the Valencia Channel outpaced that occurring at the outlet of Hirta and Vinaròs canyons. The observations noted above from Hirta Canyon suggest it may no longer be active, in which case upstream flows (mainly from Orpesa Canyon) have continued sculpting the Valencia Channel as Hirta's terminus became a hanging valley. Yet the Vinaròs Canyon appears active, so the origin of its knickpoint is more controversial. In the following section we discuss factors both upstream and downstream of the Hirta and Vinaròs junctions with the Valencia Channel that may have caused their disequilibrium form.

4.2. Controls on long-profile adjustment

4.2.1 Change in sedimentation style (upstream control)

There is abundant evidence that the Ebro margin segment of the Valencia Channel has been affected by past instability on the adjacent continental slope (Canals et al., 2000; Lastras et al., 2002, 2004; Urgeles et al., 2006). Debris flows periodically disrupted canyon tributaries south of Orpesa and buried the upper reaches of the Valencia Channel. A high-resolution seismic profile that approximately follows the uppermost course of the present Valencia Channel thalweg (Fig. 8) shows acoustically transparent seismic facies (30 ms TWT maximum thickness in the considered segment) burying a paleo-surface interpreted as the ancient Valencia Channel floor. The transparent deposit belongs to the distal end of the large BIG'95 debris flow sourced from the Ebro continental slope around 11,500 cal. yr. BP (Lastras et al., 2002). Seismic profiles nearly perpendicular to the present Valencia Channel thalweg (see tracklines in Fig. 8) reveal no significant shifting of the channel position since the debris flow event and part of the buried Valencia Channel thalweg profile (Fig. 7). Like the reaches of Vinaròs and Hirta canyons above their knickpoints, this buried profile is not concordant with the current Valencia Channel profile.

Therefore, the disruption of part of the VTTS probably caused a sudden change in sedimentation style in the upper segment of the Valencia drainage network, with a significant decrease in sediment transport and incision capacity (Fig. 9). The truncation of canyons by the source area of the BIG'95 debris flow (Lastras et al., 2004) illustrates this. Therefore, the downcutting of the Valencia Channel should be dominated by turbidity currents from the canyons draining the Catalan margin, i.e. the current Valencia Channel mid-course. This could have generated the local lowering of the base level at the termini of Hirta and Vinaròs canyons, followed by knickpoint formation. It was probably strengthened by a relative increase of the size and/or frequency of turbidity currents from Orpesa Canyon. This is clear not only from its long-profile, but also its incision into the BIG'95 debris flow described above (Fig. 8).

4.2.2. Change in spatial gradient (downstream control)

As discussed above, knickpoints in Vinaròs and Hirta canyons and the present Valencia Channel profile illustrate an "upstream" wave of erosion in the turbidite system. Interestingly, these anomalies all lay upstream of the Foix Canyon junction. No remarkable discontinuities are observed downstream along the Catalan margin (Figs. 2a and 7). Consequently, Foix Canyon and the canyons downstream stand out as key components in the Valencia drainage network.

Foix Canyon's high-relief, smooth and low-gradient slope, and a gentle junction with the Valencia Channel suggest significant sediment bypassing to the contiguous Valencia Channel. In this view, Foix Canyon is graded from turbidity current throughput that exceeds clinoform-generating background sedimentation (Case I conditions in Gerber et al., 2009). This agrees with modern sediment transfer studies that show the canyon as a preferential conduit for sediment leaving the Catalan continental shelf to the south of Barcelona (Puig and Palanques, 1998; Puig et al., 2000).

An absolute increase of turbidity current inputs to the Valencia drainage network from Foix Canyon, but also from Arenys, Besòs and Blanes canyons, might increase transport capacity and erosion rates downstream of their junctions. Given the long-profile pattern in Fig. 7, this downstream control would seem to require the development of a strong spatial gradient in downcutting rates along the Valencia Channel middle course (Fig. 9). A decrease in direct turbidite inputs from the Ebro margin to the Valencia Channel due to burial of drainage conduits, as discussed above, would further increase the gradient in transport capacity downstream of the Catalan margin inputs. Furthermore, an absolute increase in the number of flows entering directly into the Foix Canyon during glacioeustatic lowstands, when the canyon head was close to paleo-river mouths (i.e. the paleo-Llobregat River mouth), would also increase erosion capacity along the Catalan reach of the Valencia Channel (Fig. 9).

Maximum incision (370 m) of the Valencia Channel occurs after Foix Canyon junction (Fig. 2c). Cross-sections of the Valencia Channel located between canyon junctions show a clear increase in relief downstream of that junction (Fig. 4). This is also well-illustrated in seismic profiles across the Valencia Trough (Alonso et al., 1995). Most of the terraces in the Valencia Channel are observed down to the Foix junction (Figs. 3 and 7). All these observations reinforce the hypothesis that Foix Canyon drives the VTTS dynamics.

The location of the VTTS base-level has been highly variable during the Plio-Pleistocene (Palanques et al., 1994, 1995). The variation is mainly due to the internal factors described above (i.e. changes in catchment area and sediment dynamics) but also because of external ones (i.e. sediment contribution from systems outside the VTTS). Sediment is delivered to the Valencia Channel lower course from northerly sediment flows traversing the Rhône deep-sea fan and associated canyons and channels (Droz and Bellaiche, 1985; Palanques et al., 1995). Gulf of Lion cascading events also supply periodically large amounts of sediment to the deep-basin (Canals et al., 2006).

4.3. Long-term time-averaged net erosion rates

Glacio-eustatic oscillations and large sediment instability events have been identified as the likely triggers for channel migration and long-profile anomalies in the VTTS (Fig. 9). The estimated age for the last large landslide affecting the upper catchment of the VTTS is 11,500 cal. yr. BP (Lastras et al., 2002). The last lowstand episode (110–120 m below present sea level) occurred during Marine Isotope Stage (MIS) 2, about 18,000 yr BP (Waelbroeck et al., 2002).

The total incision of the Valencia Channel with respect to the projected power fits to the Vinaròs (140 m) and Hirta (60 m) canyons (Fig. 7), combined with timing for drainage network disturbance, provides estimates for time-averaged net erosion rates. If incision followed the last major landslide on the Ebro margin then the downcutting rate is 12.1 m kyr^{-1} around Vinaròs junction and 5.2 m kyr^{-1} around Hirta junction. If incision was triggered during the last glacio-eustatic lowstand then the downcutting rates are 7.7 and 3.3 m kyr^{-1}, respectively. These values should be regarded as maximum time-averaged net erosion rates because we are using the most recent events capable of triggering the channel adjustment. If the VTTS adjustment commenced during an earlier lowstand (e.g. during the MIS 4 lowstand, see Waelbroeck et al., 2002) or after an earlier landslide (e.g. Ebro margin buried landslides identified in seismic reflection profiles, see Lastras et al., 2007) we would obviously calculate slower denudation rates.

The given range of values should not be considered as pure erosion rates but rather net erosion rates. In other words, long-term time-averaging integrates many episodes of erosion and deposition. Hence, they should be regarded as maximum relief generation rates.

Turbidity currents erode the seabed through the shear stress they exert as they move over it (Pratson et al., 2000). Unfortunately, measuring turbidity currents in situ is difficult, so experimental and numerical studies are the only source of erosion rate estimates (Garcia and Parker, 1989; Kneller et al., 1999, Pratson et al., 2000, 2001). Consequently, the uncertainties concerning the scaling of laboratory-derived relationships make comparisons with natural turbid surges essentially qualitative. However, numerical models consistently show that the erosive capacity of a turbidity current tends to increase with its size or the slope length (Pratson et al., 2000; Mitchell, 2004). This is because entrainment of sediment into the current increases its momentum, which in turn increases the current's transport capacity and thus its ability to erode the bed. For reference, numerical simulations of turbidity currents by Pratson et al. (2000) suggest erosion rates of a few meters per event. Using a 3D slope stability model applied to a submarine canyon on the nearby Gulf of Lion, Sultan et al. (2007) suggested that slope instabilities and reshaping of canyon walls can be triggered after only 5 m of axial incision.

Thus, it is reasonable to expect high long-term erosion rates caused by repeated turbidity currents in the Valencia Channel in light of the observed size of the drainage network, the outstanding relief and width of the Valencia Channel in its middle-course (Fig. 2), the development of extensive levees along the lower course (Alonso et al., 1995) and the extension of the Valencia Fan (Palanques et al., 1994). Furthermore, it is also remarkable the morphologic inconsistency between the buried long-profile of the ancient Valencia Channel upper course (Fig. 7) and the present profile, which again points to drastic channel adjustment after the occurrence of the BIG'95 debris flow at the Ebro margin. The terminal Valencia Lobe (Droz et al., 2006), which extends more than 150 km downdip on the Algero-Balearic abyssal plain east of the Minorca Island, also records the activity of the Valencia Channel in fresh bedforms and erosional features as well as layers containing pteropod shells of Holocene age (Morris et al., 1998). At this stage the extent to which these fresh bedforms and erosional features are attributable to repeated turbidity currents and not the frequent highstand cascades of dense shelf water is unknown (Canals et al., 2006; Gaudin et al., 2006). Direct evidence of long-term erosion in the Valencia Channel was observed during Deep Sea Drilling Project Leg 13 site 122 (Ryan et al., 1973), located very close to the middle-course of the current thalweg (Figs. 1 and 4). Sediments recovered from the borehole showed a late-middle Quaternary coarse-grained top unit directly overlying Upper Pliocene sediments (Ryan et al., 1973). The time-gap estimated for the unconformity is at least one million years.

5. Conclusions

The analysis of along-thalweg depth profiles (i.e. long-profiles) in turbidite systems yields information about the sedimentary history of a submarine basin. In the present study we examine long-profiles to address the long-term evolution of the Valencia Trough turbidite system (VTTS).

The VTTS is unique because it drains sediment from different margin morpho-types that share a common final conduit, the Valencia Channel. This margin-to-margin interconnection allows the propagation of local effects through the whole system. The integrated analysis of turbidite channel long-profiles shows evidence for transient incision in the VTTS in the form of a knickpoint in Vinaròs Canyon and a hanging tributary in Hirta Canyon. Based on the location and form of these morphologies we identify two main triggering mechanisms that may have caused their disequilibrium form: (1) a change in sedimentation style forced by a large debris flow at 11,500 yr BP that disrupted the upper reaches of the VTTS, and (2) a change in downcutting rates along the Valencia Channel middle course due to shifting sediment input during glacio-eustatic lowstands. From our morphometric observations, we conclude that the South Catalan canyons, especially Foix Canyon, played a key role in the drainage dynamics of the VTTS.

Long-term time-averaged Valencia Channel incision rates have been estimated based on the two incision triggering mechanisms inferred above. From assumed dates for the onset of incision in these two scenarios, incision rates around the Vinaròs junction are from 7.7 to 12.1 m kyr^{-1}, while near Hirta junction are from 3.3 to 5.2 m kyr^{-1}. These values should be taken as rough estimates for maximum relief generation rates in the submarine channel.

In this paper we have shown how new detailed bathymetry across an entire basin provides clues to the evolution of submarine drainage networks shaped primarily by the action of turbidity currents. Like studies of landscape evolution from DEMs, our work makes inferences about seascape evolution from high-quality bathymetry. Even in the absence of extensive subsurface data, much can be learned about recent basin evolution from detailed observations of the modern seascape.

Acknowledgements

This research was supported by the HERMIONE project, EC contract 226354-HERMIONE, funded by the European Commission's Seventh Framework Programme, and the HERMES Project, EC contract GOCE-CT-2005-511234, funded by the European Commission's Sixth Framework Programme under the priority “Sustainable Development, Global Change and Ecosystems”. It has also benefited from inputs by the PROMETEO (CTM2007-66316-C02-01/MAR), EDINSED3D (CTM2007-64880/MAR), and the GRACCIE CONSOLIDER (CSD2007-00067) projects, both funded by the Spanish RTD Programme. GRC Geociències Marines is supported by Generalitat de Catalunya “Grups de Recerca Consolidats” grant 2009 SGR 1305. The paper was substantially improved by constructive reviews by P.P. Cunha and editor T. Oguchi.

References

Adeogba, A.A., McHargue, T.R., Graham, S.A., 2005. Transient fan architecture and depositional controls from near-surface 3-D seismic data, Niger Delta continental slope. Am. Assoc. Pet. Geol. Bull. 89, 627-643.

Alonso, B., Field, M.E., Gardner, J.V., Maldonado, A., 1990. Sedimentary evolution of the Pliocene Ebro margin, northeastern Spain. Mar. Geol. 95, 313-331.

Alonso, B., Canals, M., Got, H., Maldonado, A., 1991. Seavalleys and related depositional systems in the Catalan Sea (northwestern Mediterranean Sea). Am. Assoc. Pet. Geol. Bull. 75, 1195-1214.

Alonso, B., Canals, M., Palanques, A., Rehault, J.P., 1995. A deep-sea channel in the northwestern Mediterranean Sea: Morphology and seismic structure of the Valencia Channel and its surroundings. Mar. Geophys. Res. 17, 469-484.

Amblas, D., Canals, M., Lastras, G., Berné, S., Loubrieu, B., 2004. Imaging the seascapes of the Mediterranean. Oceanography 17(4), 144-155.

Amblas, D., Canals, M., Urgeles, R., Lastras, G., Hughes-Clarke, J.E., 2006. Morphogenetic mesoscale analysis of the northeastern Iberian margin, NW Mediterranean basin. Mar. Geol. 234, 3-20.

Berné, S., Loubrieu, B., CALMAR Ship-board Party, 1999. Canyons et processus sédimentaires récents sur la Marge Occidentale du Golfe du Lion. Premiers Résultats de la Campagne Calmar. C.R. Acad. Sci. 328, 471-477.

Bouma, A., Normark, W. R., Barnes, N. E., 1986. Submarine Fans and Related Turbidite Systems. Springer Verlag, New York.

Boyd, R., Ruming, K., Goodwin, I., Sandstrom, M., Schröder-Adams, C., 2008. Highstand transport for coastal sand to the deep ocean: a case study from Fraser Island, southeast Australia. Geology 36, 15-18.

Canals, M., Alonso, B., Baraza, J., Ercilla, G., Calafat, A.M., Masson, D.G., Farran, M., Sorribas, J., Estrada, F., Cavaller, M., Prieto, M.J., Rodríguez, J.P., Maillard, N., 1995. Estudio oceanográfico multidisciplinar del Mar Catalano-Balear; Informe de la Campaña BIG 95. Cruise report (in Spanish, with English Abstr.). Universitat de Barcelona, Barcelona, Spain, 94 pp.

Canals, M., Casamor, J.L., Urgeles, R., Lastras, G., Calafat, A.M., De Batist, M., Masson, D., Berné, S., Alonso, B., Hughes-Clarke, J.E., 2000. The Ebro continental margin, Western Mediterranean Sea: Interplay between canyon-channel systems and mass wasting processes. In: Nelson, C.H., Weimer, P. (Eds.), Deep-water Reservoirs of the World: GCSSEPM Foundation 20th Annual Research Conference, Houston, Texas, pp.152-174 (CD edition).

Canals, M., Puig, P., Durrieu de Madron, X., Heussner, S., Palanques, A., Fabres, J., 2006. Flushing submarine canyons. Nature 444, 354-357.

Cattaneo, A., Trincardi, F., Langone, L., Asioli, A., Puig, P., 2004. Clinoform generation on Mediterranean margins. Oceanography 17(4), 105-117.

Cita, M.B., Ryan, W.B.F., Kidd, R.B., 1978. Sedimentation rates in Neogene deep-sea sediments from the Mediterranean and geodynamic implications of their change. In: Hsü, K.J., Montadert, L., and others (Eds.). Initial Reports of the Deep Sea Drilling Project 42, Part I, Government Printing Office, Washington D.C., pp. 991-1002.

Cook, K.L., Whipple, K.X., Heimsath, A.M., Hanks, T.C., 2009. Rapid incision of the Colorado River in Glen Canyon – insights from channel profiles, local incision rates, and modeling of lithologic controls. Earth Surf. Process. Landforms 34, 994–1010.

Covault, J.A., Romans, B.W., 2009. Growth patterns of deep-sea fans revisited: Turbidite-system morphology in confined basins, examples from the California Borderland. Mar. Geol. 265, 51-66.

Crosby, B.T., Whipple, K.X., 2006. Knickpoint initiation and distribution within fluvial networks: 236 waterfalls in the Waipaoa River, North Island, New Zealand. Geomorphology 82, 16.38.

Dana, J.D., 1863. Manual of Geology: Treating of the Principles of the Science with Special Reference to American Geological History, for the Use of Colleges, Academies, and Schools of Science. Theodore Bliss & Co., Philadelphia, 798 pp.

Droz, L., Bellaiche, G., 1985. Rhône Deep-sea Fan: morphostructure and growth pattern. Am. Assoc. Pet. Geol. Bull. 69, 460-479.

Droz, L., dos Reis, A.T., Rabineau, M., Berné, S., Bellaiche, G., 2006. Quaternary turbidite systems on the northern margins of the Balearic Basin (Western Mediterranean): a synthesis. Geo-Mar. Lett. 26, 347-359.

Field, M.E., Gardner, J.V., 1990. Pliocene-Pleistocene growth of the Rio Ebro margin, northeast Spain: a prograding-slope model. Geol. Soc. Am. Bull. 102, 721-733.

Garcia, M., Parker, G., 1989. Experiments on hydraulic jumps in turbidity currents near a canyon-fan transition. Science 245(4916), 393-396.

Gaudin, M., Berné, S., Jouanneau, J.M., Palanques, A., Puig, P., Mulder, T., Cirac, P., Rabineau, M., Imbert, P., 2006. Massive sand beds attributed to deposition by dense water cascades in the Bourcart canyon head, Gulf of Lions (northwestern Mediterranean Sea). Mar. Geol. 234, 111-128.

Gerber, T.P., Amblas, D., Wolinsky, M.A., Pratson, L.F., Canals, M., 2009. A model for the long-profile shape of submarine canyons. J. Geophys. Res. 114, F03002.

Howard, A.D., Dietrich, W.E., Seidl, M.A., 1994. Modeling fluvial erosion on regional to continental scales. J. Geophys. Res. 99, 13971-13986.

Kertznus, V., Kneller, B., 2009. Clinoform quantification for assessing the effects of external forcing on continental margin development. Basin Res. 21, 738–758.

Kneller, B. C., Bennett, S.J., McCaffrey, W.D., 1999. Velocity structure, turbulence and fluid stresses in experimental gravity currents. J. Geophys. Res. 104(C3), 5381-5391.

Kneller, B., 2003. The influence of flow parameters on turbidite slope channel architecture. Mar. Petrol. Geol. 20, 901-910.

Lastras, G., Canals, M., Hughes-Clarke, J.E., Moreno, A., De Batist, M., Masson, D.G., Cochonat, P., 2002. Seafloor imagery from the BIG'95 debris flow, western Mediterranean. Geology 30, 871-874.

Lastras, G., Canals, M., Urgeles, R., De Batist, M., Calafat, A.M., Casamor, J.L., 2004. Characterisation of the recent BIG'95 debris flow deposit on the Ebro margin, Western Mediterranean Sea, after a variety of seismic reflection data. Mar. Geol. 213, 235-255.

Lastras, G., Canals, M., Amblas, D., Frigola, J., Urgeles, R., Calafat, A.M., Acosta, J., 2007. Slope instability along the northeastern Iberian and Balearic continental margins. Geol. Acta 5, 35-47.

Lastras, G., Canals, M., Amblas, D., Lavoie, C., Church, I., De Mol, B., Duran, R., Calafat, A.M., Hughes-Clarke, J.E., Smith, C., Heussner, S., Euroleón cruise shipboard party, 2011. Geomorphology of Blanes and La Fonera canyon heads, western Mediterranean Sea. Mar. Geol. doi:10.1016/j.margeo.2010.11.005.

Maillard, A., Mauffret, A., 1999. Crustal structure and riftogenesis of the Valencia Trough (north-western Mediterranean Sea). Basin Res. 11, 357-379.

Maillard, A., Gorini, C., Mauffret, A., Sage, F., Lofi, J., Gaullier, V., 2006. Offshore evidence of polyphase erosion in the Valencia Basin (Northwestern Mediterranean): Scenario for the Messinian Salinity Crisis. Sediment. Geol. 188-189, 69-91.

Mitchell, N.C., 2004. Form of submarine erosion from confluences in Atlantic USA Continental Slope canyons. Am. J. Sci. 304, 590–611.

Mitchell, N.C., 2005a. Interpreting long-profiles of canyons in the USA Atlantic continental slope. Mar. Geol. 214, 75-99.

Mitchell, N.C., 2005b. Erosion of canyons in continental slopes. In: Hodgson, D.M., Flint, S.S. (Eds.), Submarine Slope Systems; Processes and Products. Geological Society Special Publications 244, London, pp. 131-140.

Mitchell, N.C., 2006. Morphologies of knickpoints in submarine canyons. GSA Bull. 118, 589-605.

Mitchell, N.C., Dade, W.D., Masson, D.G., 2003. Erosion of the submarine flanks of the Canary Islands. J. Geophys. Res. 108 (F1), 6002. doi:10.1029/2002JF000003.

Mitchum, R.M.Jr., Vail, P.R., Sangree, J.B., 1977. Seismic stratigraphy and global changes of sea levels, part 6: stratigraphic interpretation of seismic reflection patterns in depositional sequences: in Payton, C.E. (Ed.), Seismic Stratigraphy Applications to Hydrocarbon Exploration, AAPG Memoir 26, pp. 117-133.

Morris, S.A., Kenyon, N.H., Limonov, A.F., Alexander, J., 1998. Downstream changes of large-scale bedforms in turbidites around the Valencia channel mouth, north-west Mediterranean: implications for palaeoflow reconstruction. Sedimentology 45, 365-377.

Niemann, J.D., Gasparini, N.M., Tucker, G.E., Bras, R.L., 2001. A quantitative evaluation of Playfair’s Law and its use in testing long-term stream erosion models. Earth Surf. Process. Landforms 26, 1317-1332.

Nittrouer, C.A., Kuehl, S.A., DeMaster, D.J., Kowsmann, R.O., 1986. The deltaic nature of Amazon shelf sedimentation. GSA Bull. 97, 444-458.

Normark, W.R., 1970. Growth patterns of deep-sea fans. Am. Assoc. Pet. Geol. Bull. 54, 2170-2195.

Olley, J.M., Pietsch, T., Roberts, R.G., 2004. Optical dating of Holocene sediment from a variety of geomorphic settings using single grains of quartz. Geomorphology 60, 337-358.

Palanques, A., Maldonado, A., 1985. Sedimentology and evolution of the Valencia Valley and Fan (Northwestern Mediterranean). Acta Geol. Hisp. 20, 1-19.

Palanques, A., Alonso, B., Farrán, M., 1994. Progradation and retreat of the Valencia fanlobes controlled by sea level changes during the Plio-Pleistocene (Northwestern Mediterranean). Mar. Geol. 117, 195-205.

Palanques, A., Kenyon, N.H., Alonso, B., Limonov, A., 1995. Erosional and Depositional Patterns in the Valencia channel Mouth: An example of a Modern Channel-Lobe Transition Zone. Mar. Geophys. Res. 17, 503-517.

Petter, A.L., Kim, W., Muto, T., Steel, R.J., 2011. Comment on 'Clinoform quantification for assessing the effects of external forcing on continental margin development'. Basin Res. 23, 118-121.

Pirmez, C., Beaubouef, R.T. Friedmann, S.J., Mohrig, D.C., 2000. Equilibrium profile and baselevel in submarine channels: examples from Late Pleistocene systems and implications for the architecture of deep water reservoirs. In: Weimar, P., Slatt, R.M., Coleman, J., Rosen, N.C., Nelson, H., Bouma, A.H., Styzen, M.J., Lawrence, D.T. (Eds.), Deep-water Reservoirs of the World. GCSSEPM Foundation 20th Annual Research Conference, pp. 782-805.

Pirmez, C., Imran, J., 2003. Reconstruction of turbidity currents in Amazon Channel. Mar. Petrol. Geol. 20, 823-849.

Playfair, J., 1802. Illustrations of the Huttonian Theory of the Earth. Cadell and Davies, London, and Greech, Edinburgh.

Pratson, L.F., Imran, J., Parker, G., Syvitski, J.P.M., Hutton, E., 2000. Debris Flows vs. Turbidity Currents: a Modeling Comparison of Their Dynamics and Deposits. In: Bouma, A.H., Stone, C.G. (Eds.), Fine-grained Turbidite Systems. Am. Assoc. Pet. Geol. Memoir 72/SEPM Special Publication 68, pp. 57-72.

Pratson, L.F., Imran, J., Hutton, E.W.H., Parker, G., Syvitski, J.P.M., 2001. BANG1D: a one-dimensional, Lagrangian model of subaqueous turbid surges. Comput. Geosci. 27(6), 701-716. doi:10.1016/S0098-3004(00)00123-0.

Pratson, L.F., Nittrouer, C.A., Wiberg, P.L., Steckler, M.S., Swenson, J.B., Cacchione, D.A., Karson, J.A., Murray, A.B., Wolinsky, M.A., Gerber, T.P., Mullenbach, B.L., Spinelli, G.A., Fulthorpe, C.S., O'Grady, D.B., Parker, G., Driscoll, N.W., Burger, R.L., Paola, C., Orange, D.L., Field, M.E., Friedrichs, C.T., Fedele, J.J., 2009. Seascape evolution on clastic continental shelves and slopes. In: Nitrouer, C.A., Austin, J.A., Field, M.E., Kravitz, J.H., Syvitski, J.P.M., Wiberg, P.L., (Eds.), Continental-Margin Sedimentation: From Sediment Transport to Sequence Stratigraphy. IAP Special Publication 37, Blackwell Publishing, Oxford, pp. 339-380.

Puig, P., Palanques, A., 1998. Nepheloid structure and hydrographic control on the Barcelona continental margin, NW Mediterranean. Mar. Geol. 149, 39-54.

Puig, P., Palanques, A., Guillen, J., Garcia-Ladona, E., 2000. Deep slope currents and suspended particle fluxes in and around the Foix submarine canyon (NW Mediterranean). Deep-Sea Res. 47, 343-366.

Rabineau, M., Berne, S., Aslanian, D., Olivet, J.L., Joseph, P., Guillocheau, F., 2005. Sedimentary sequences in the Gulf of Lion: A record of 100,000 years climatic cycles. Mar. Petrol. Geol. 22, 775-804.

Roca, E., Sans, M., Cabrera, L., Marzo, M., 1999. Oligocene to Middle Miocene evolution of the central Catalan margin (northwestern Mediterranean). Tectonophysics 315, 209-233.

Ryan, W.B.F, Hsü, K.J., Cita, M.B., Dumitrica, P., Lort, J., Maync, W., Nesteroff, W.D., Pautot, G., Stradner, H., Wezel, F.C., 1973. Valencia Trough, site 122. DSDP Leg 13 site 122 Report, 91-109.

Sultan, N., M. Gaudin, S. Berne, M. Canals, R. Urgeles, Lafuerza, S., 2007. Analysis of slope failures in submarine canyon heads: an example from the Gulf of Lions. J. Geophys. Res. 112, F01009. doi:10.1029/2005fj000408.

Shepard, F.P., 1981. Submarine canyons; multiple causes and long-time persistence. Am. Assoc. Pet. Geol. Bull. 65, 1062–1077.

Urgeles, R., Leynaud, D., Lastras, G., Canals, M., Mienert, J., 2006. Back-analysis and failure mechanisms of a large submarine slide on the Ebro continental slope, NW Mediterranean. Mar. Geol. 226, 185-206.

Urgeles, R., Camerlenghi, A., Garcia-Castellanos, D., De Mol, B., Garcés, M., Vergés, J., Haslam, I., Hardman, M., 2010. New constraints on the Messinian sealevel drawdown from 3D seismic data of the Ebro Margin, western Mediterranean. Basin Res. doi:10.1111/j.1365-2117.2010.00477.x.

Waelbroeck, C., Labeyrie, L., Michel, E., Duplessy, J.C., McManus, J.F., Lambeck, K., Balbon, E., Labracherie, M., 2002. Sea-level and deep water temperature changes derived from benthic foraminifera isotopic records. Quaternary Sci. Rev. 21, 295–305.

Whipple, K.X., Tucker, G.E., 2002. Implications of sediment-flux-dependent river incision models for landscape evolution. J. Geophys. Res. 107(B2), 2039. doi:10.1029/2000JB000044.

Figure captions

Fig. 1. DTM of the study area. Illumination is from the NE. Elevation data are a combination of different multibeam data sets and global digital databases. The white dashed lines follow the axis of the main Valencia drainage network. BlC, Blanes Canyon; AC, Arenys Canyon; BeC, Besòs Canyon; FC, Foix Canyon; ViC, Vinaròs Canyon; HiC, Hirta Canyon; OrC, Orpesa Canyon; CGC, Columbretes Grande Canyon; RDSF, Rhône Deep-Sea Fan; DPCSB, Deep Pyrenean Canyons Sedimentary Body; WDF, Western Debris Flow; BDF, BIG'95 Debris Flow. White capital letters (A-F) near canyon junctions with the Valencia Channel show the location of the bathymetric zooms displayed in Fig. 3. Black dotted boxes show location of Figs. 4, 5 and 8.

Fig. 2. Elevation-distance plots for the Valencia Trough turbidite systems. **a)** Longitudinal profiles of the main submarine valleys feeding the Valencia Channel from the southernmost modern tributary (Orpesa) to the Valencia Fan (distal end of plot) extracted from swath bathymetry (50 m grid resolution). Gray dotted curve is the smoothed bathymetric profile of the Valencia Channel margin parallel to its thalweg. Gray dotted box shows limits of Fig. 7. Vertical dashed lines (A–F) mark junctions of canyons with the Valencia Channel (see Fig. 3). **b)** Valencia Channel long-profile plotted with its elevation power-law fit (dotted curve) and the gradient of that fit (gray curve). **c)** Valencia Channel relief profile measured along the northern margin of the channel, and channel width measurements taken every 10 km (gray curve).

Fig. 3. 3D perspective view of canyon junctions (A-F) with the Valencia Channel (at 4x vertical exaggeration). Key features are labeled, as well as the location (in A) of the seismic line shown in Fig. 8. Terraces in the Valencia Channel are also indicated (T1–T8).

Fig. 4. Bathymetric cross-sections of the Valencia Channel between canyon junctions. See Fig. 1 for location. ValCh, Valencia Channel; BlC, Blanes Canyon; AC, Arenys Canyon; BeC, Besòs Canyon; FC, Foix Canyon; ViC, Vinaròs Canyon; HiC, Hirta Canyon; OrC, Orpesa Canyon.

Fig. 5. Vinaròs canyon junction with the Valencia Channel. See Fig. 1 for location. **a and b)** 30 kHz TOBI side-scan sonographs draped on multibeam bathymetry data. **c)** Main geomorphic features including the Vinaròs Knickpoint and the Valencia Channel terrace T2.

Fig. 6. Distance-relief plots normalized by the total relief (from canyon head to the junction with the Valencia Channel) for submarine canyons draining into the Valencia Channel. Local relief is computed from a best-fit surface to inter-canyon margin profiles. The plots highlight differences in the amount of canyon entrenchment.

Fig. 7. Zoom of the upper and middle course of the Valencia drainage network (see Fig. 2a for location) showing interpreted features of canyon-channel long-profiles. For Hirta and Vinaròs canyons, dashed lines show power-law fits to profiles above knickpoints that are projected below the knickpoints and down the Valencia axis. Also shown is a power-law fit to the Orpesa and Valencia combined long-profile. Black dotted line shows the location of the buried (by the BIG'95 debris flow) Valencia Channel profile upper course measured from high-resolution seismic reflection profiles nearly perpendicular to the present Valencia Channel thalweg (see seismic survey tracklines in Fig. 8). Terraces (T1–T8) observed along the Valencia Channel are also indicated.

Fig. 8. Very high resolution seismic reflection profile showing the distal deposit of the BIG'95 debris flow covering a surface (dotted line) interpreted as a former upper thalweg of the Valencia Channel. See Fig. 1 for location. Red line in the location box shows the position of the seismic profile, while the black dotted lines show the rest of the seismic survey navigation in the selected zone.

Fig. 9. Cartoon illustrating the conceptual model for transient profile adjustment triggered by upstream (**a**) and downstream (**b**) controls. In both cases, the relative flow throughput (i.e. flow-event frequency) at different parts of the Valencia Channel is represented. In (a), the trigger mechanism is a decrease in flow throughput (time 2) along the Ebro reach of the Valencia Channel following the disruption and burial of the upper reaches of the VTTS by a submarine debris flow. In (b), the profile is adjusted by increased flow throughput (time 2) during sealevel lowstands along the South Catalan Margin (SCM) reach of the Valencia Channel, when canyon heads are close to river mouths. The vertical thickness of the flow throughput wedges is proportional to relative flow-event frequency.

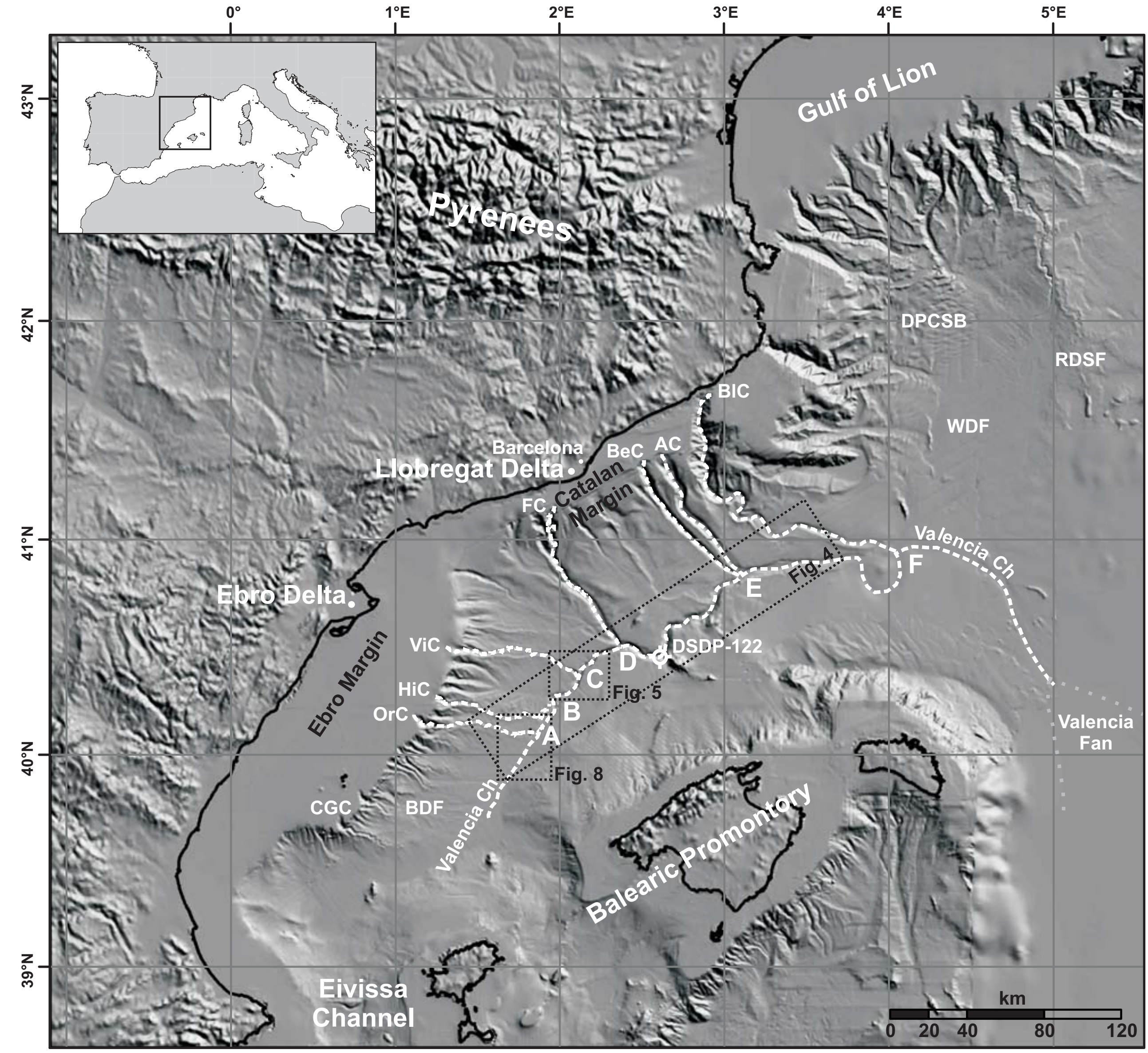

0°
1°E
2°E
3°E
4°E
5°E
43°N
42°N
41°N
40°N
39°N
Gulf of Lion
Pyrenees
DPCSB
RDSF
WDF
BIC
BeC
AC
Barcelona
Llobregat Delta
Catalan Margin
FC
Valencia Ch
F
E
Fig. 4
Ebro Delta
ViC
D
DSDP-122
C
Fig. 5
HiC
OrC
B
A
Ebro Margin
Fig. 8
Valencia Fan
CGC
BDF
Valencia Ch
Balearic Promontory
Eivissa Channel
km
0 20 40 80 120

Fig.1

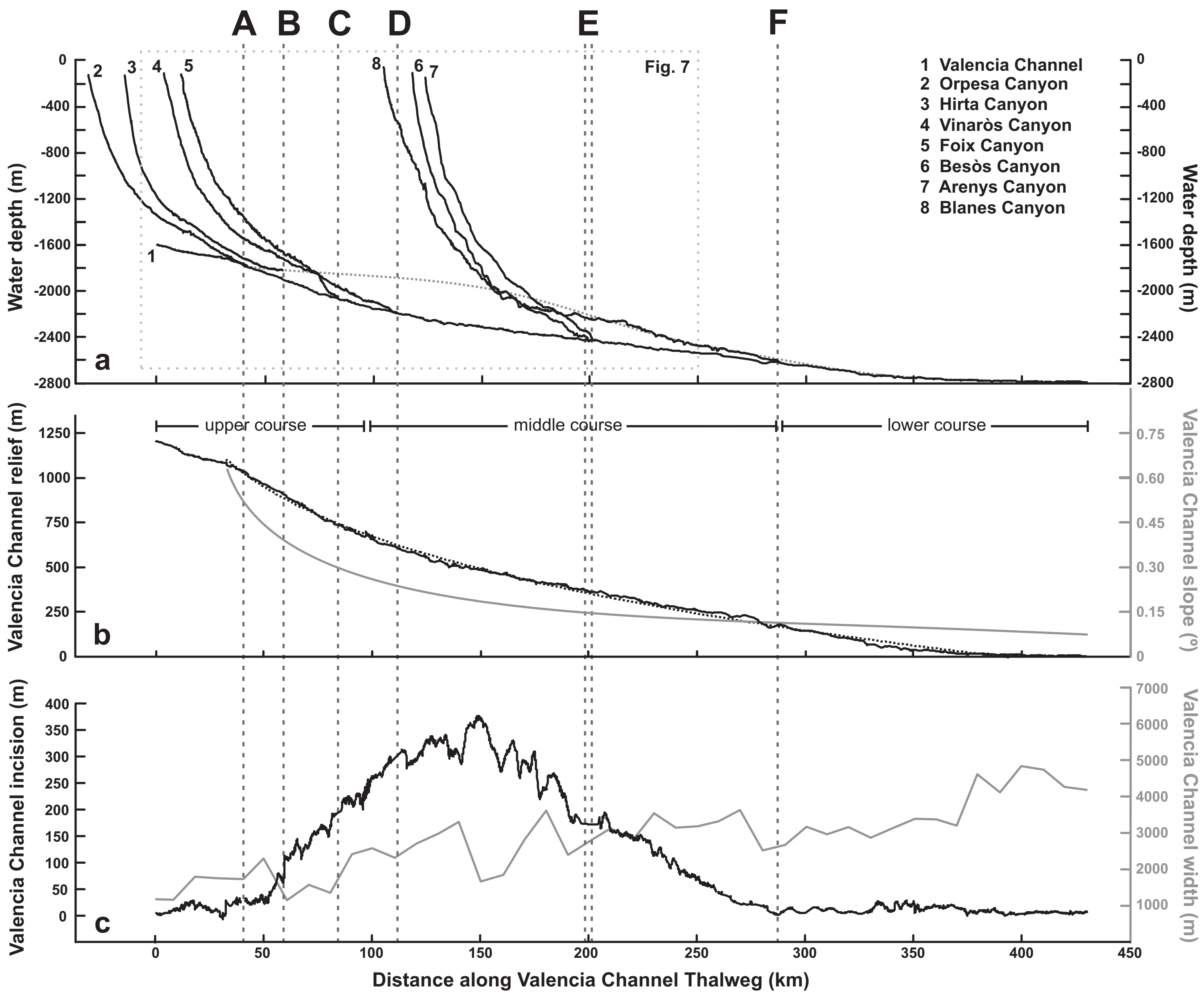

A
B
C
D
E
F
Fig. 7
1 Valencia Channel
2 Orpesa Canyon
3 Hirta Canyon
4 Vinaròs Canyon
5 Foix Canyon
6 Besòs Canyon
7 Arenys Canyon
8 Blanes Canyon
Water depth (m)
a
upper course
middle course
lower course
Valencia Channel relief (m)
Valencia Channel slope (°)
b
Valencia Channel incision (m)
Valencia Channel width (m)
c
Distance along Valencia Channel Thalweg (km)

Fig.2

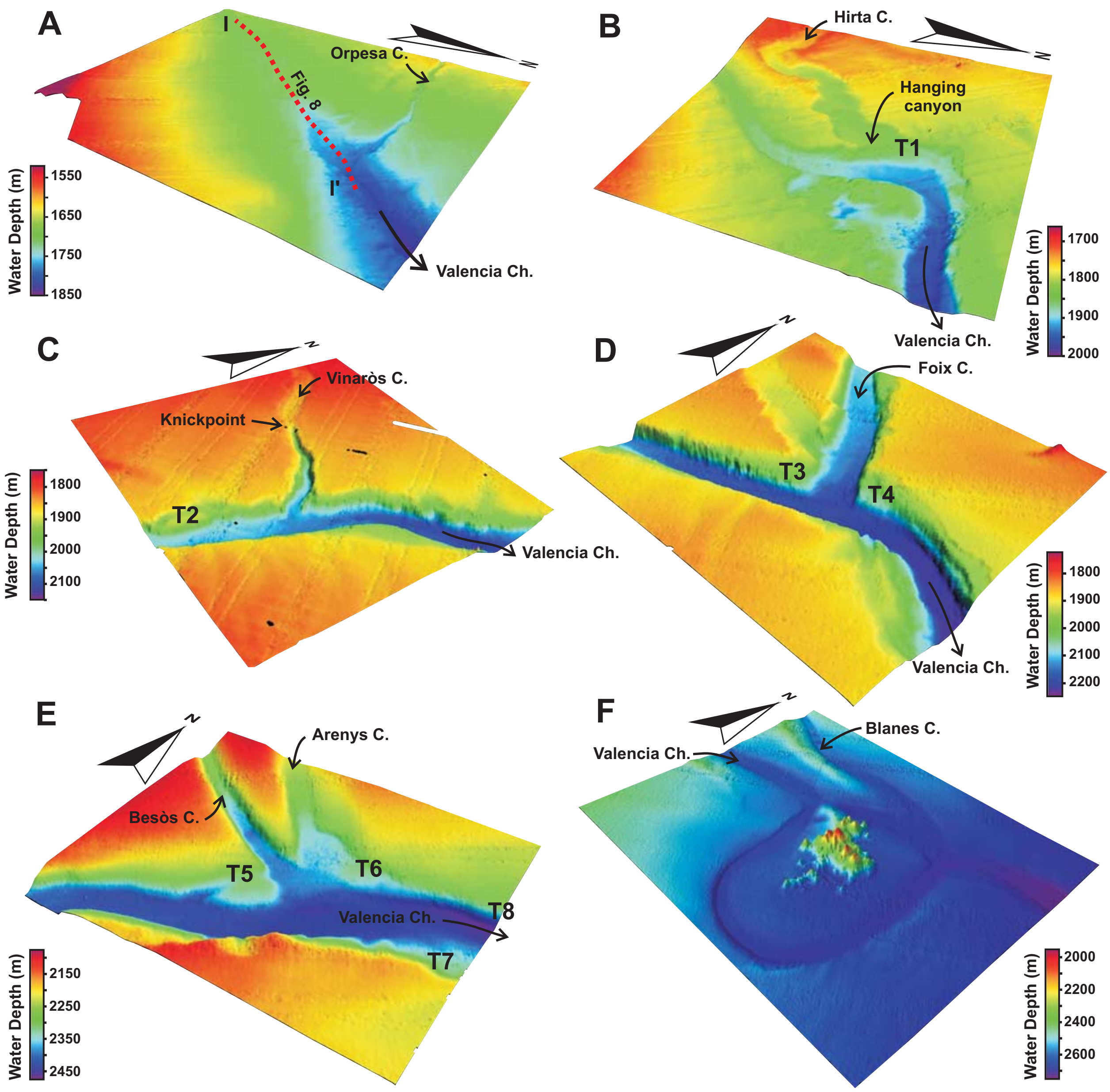
A
I
Orpesa C.
Fig. 8
I'
Valencia Ch.
Water Depth (m)
1550
1650
1750
1850
B
Hirta C.
Hanging canyon
T1
Valencia Ch.
Water Depth (m)
1700
1800
1900
2000
C
Vinaròs C.
Knickpoint
T2
Valencia Ch.
Water Depth (m)
1800
1900
2000
2100
D
Foix C.
T3
T4
Valencia Ch.
Water Depth (m)
1800
1900
2000
2100
2200
E
Arenys C.
Besòs C.
T5
T6
Valencia Ch.
T8
T7
Water Depth (m)
2150
2250
2350
2450
F
Valencia Ch.
Blanes C.
Water Depth (m)
2000
2200
2400
2600

Fig.3

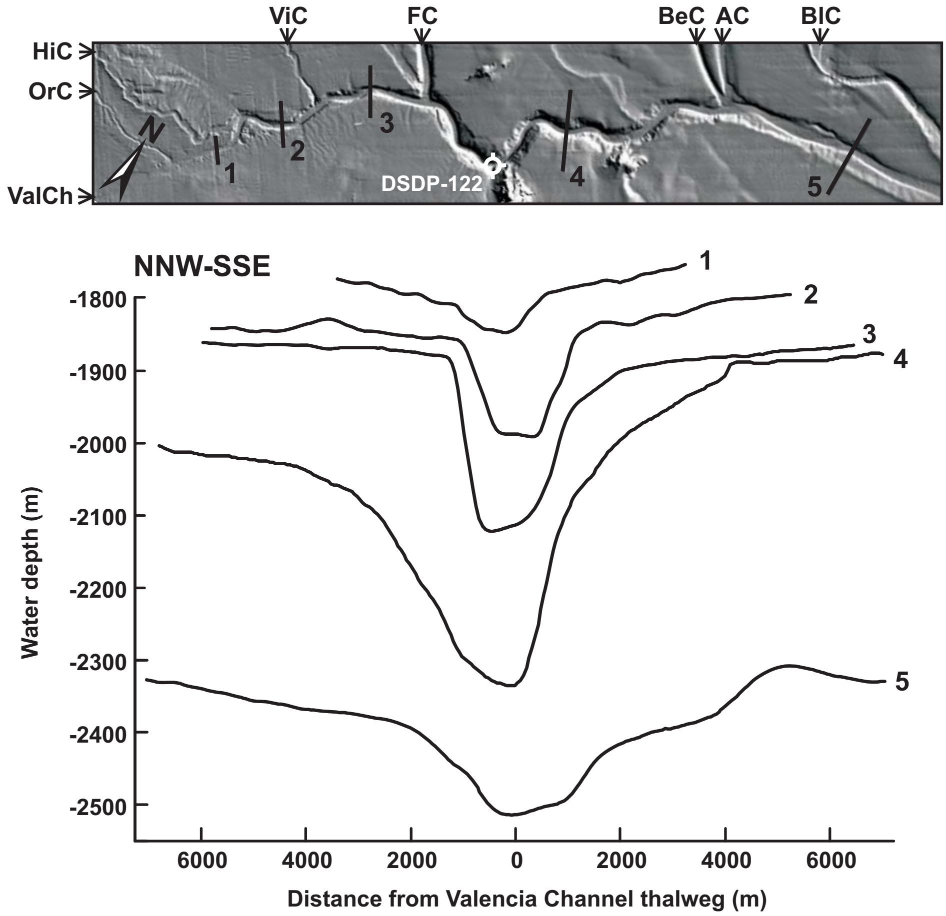
ViC
FC
BeC
AC
BlC
HiC
OrC
ValCh
N
1
2
3
4
5
DSDP-122
NNW-SSE
-1800
-1900
-2000
-2100
-2200
-2300
-2400
-2500
Water depth (m)
6000
4000
2000
0
2000
4000
6000
Distance from Valencia Channel thalweg (m)

Fig.4

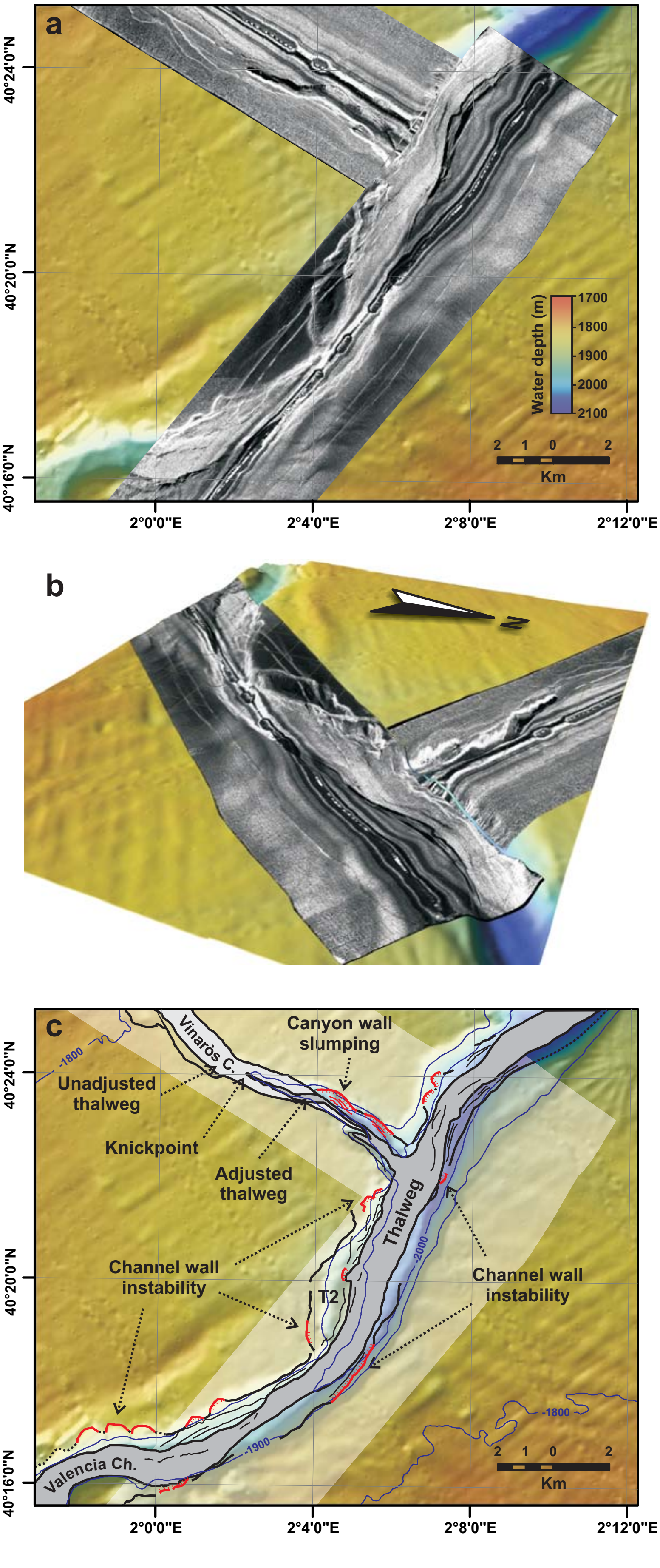
a
40°24'0"N
40°20'0"N
40°16'0"N
2°0'0"E
2°4'0"E
2°8'0"E
2°12'0"E
Water depth (m)
1700
1800
1900
2000
2100
2 1 0 2
Km
b
N
c
Vinaròs C.
Canyon wall slumping
Unadjusted thalweg
Knickpoint
Adjusted thalweg
Thalweg
Channel wall instability
Channel wall instability
T2
Valencia Ch.
-1800
-1900
-2000

Fig.5

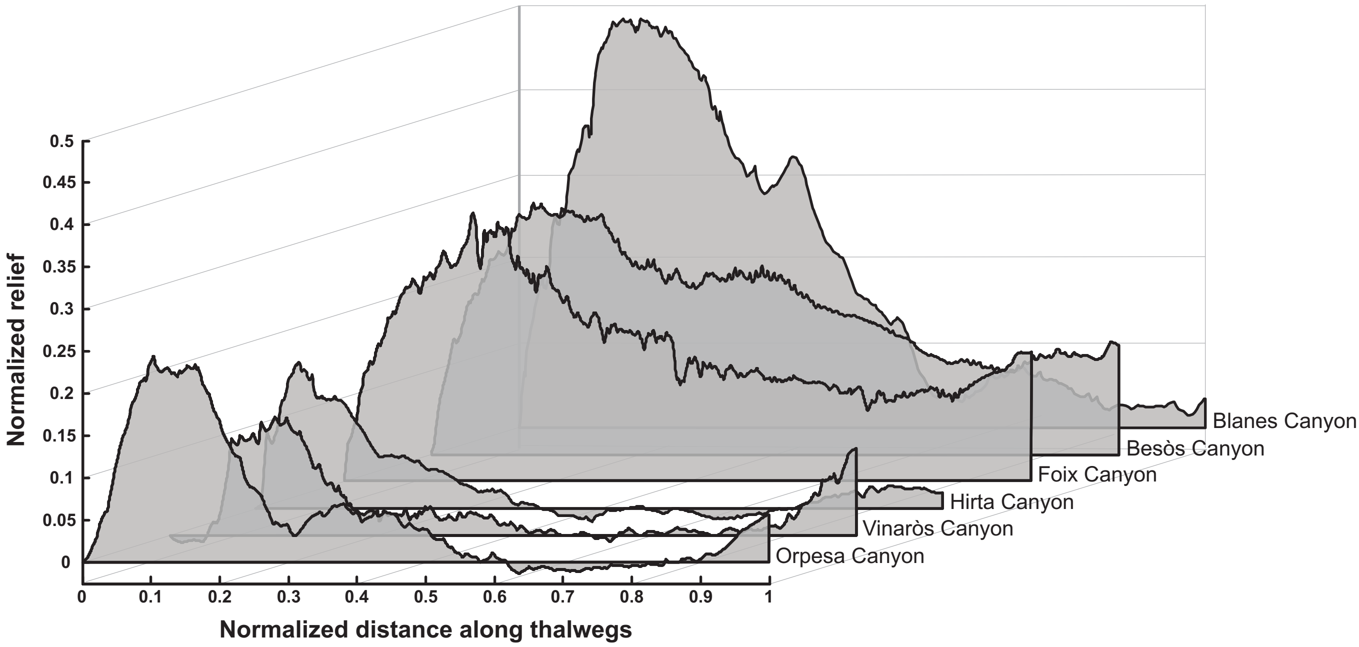

Normalized relief
0.5
0.45
0.4
0.35
0.3
0.25
0.2
0.15
0.1
0.05
0
0
0.1
0.2
0.3
0.4
0.5
0.6
0.7
0.8
0.9
1
Normalized distance along thalwegs
Blanes Canyon
Besòs Canyon
Foix Canyon
Hirta Canyon
Vinaròs Canyon
Orpesa Canyon

Fig.6

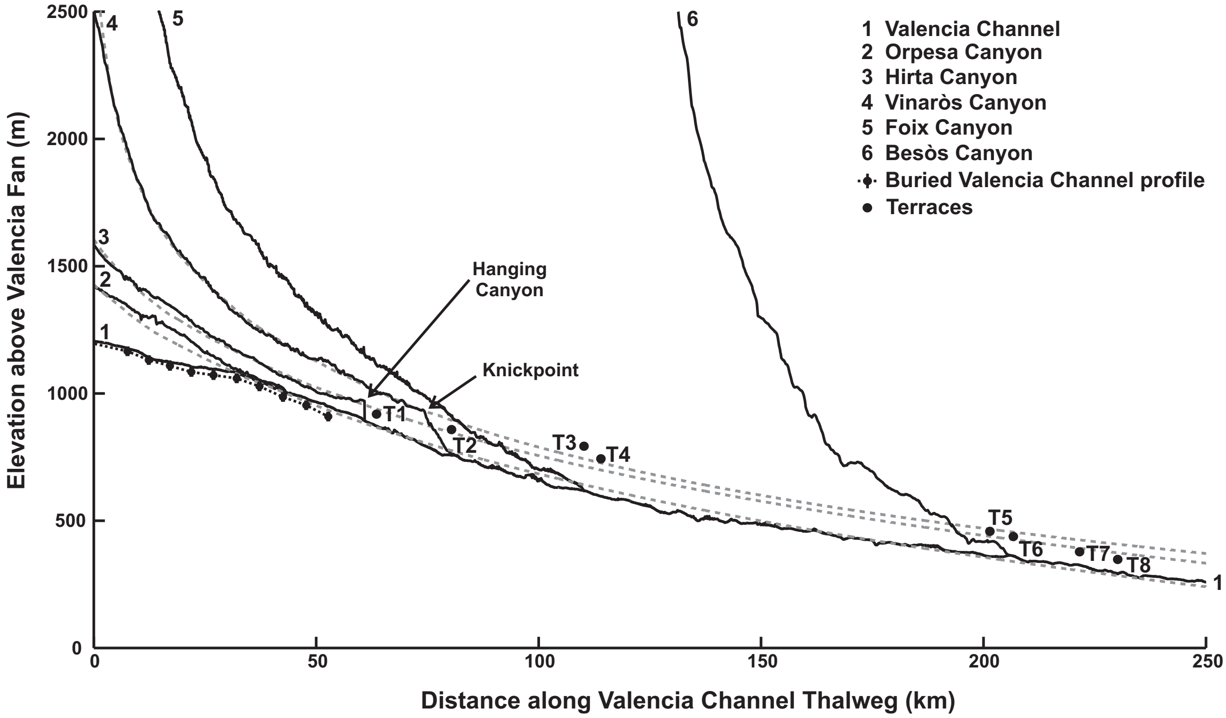
1 Valencia Channel
2 Orpesa Canyon
3 Hirta Canyon
4 Vinaròs Canyon
5 Foix Canyon
6 Besòs Canyon
Buried Valencia Channel profile
Terraces
Hanging Canyon
Knickpoint
T1
T2
T3
T4
T5
T6
T7
T8
Elevation above Valencia Fan (m)
Distance along Valencia Channel Thalweg (km)
0
500
1000
1500
2000
2500
0
50
100
150
200
250

Fig.7

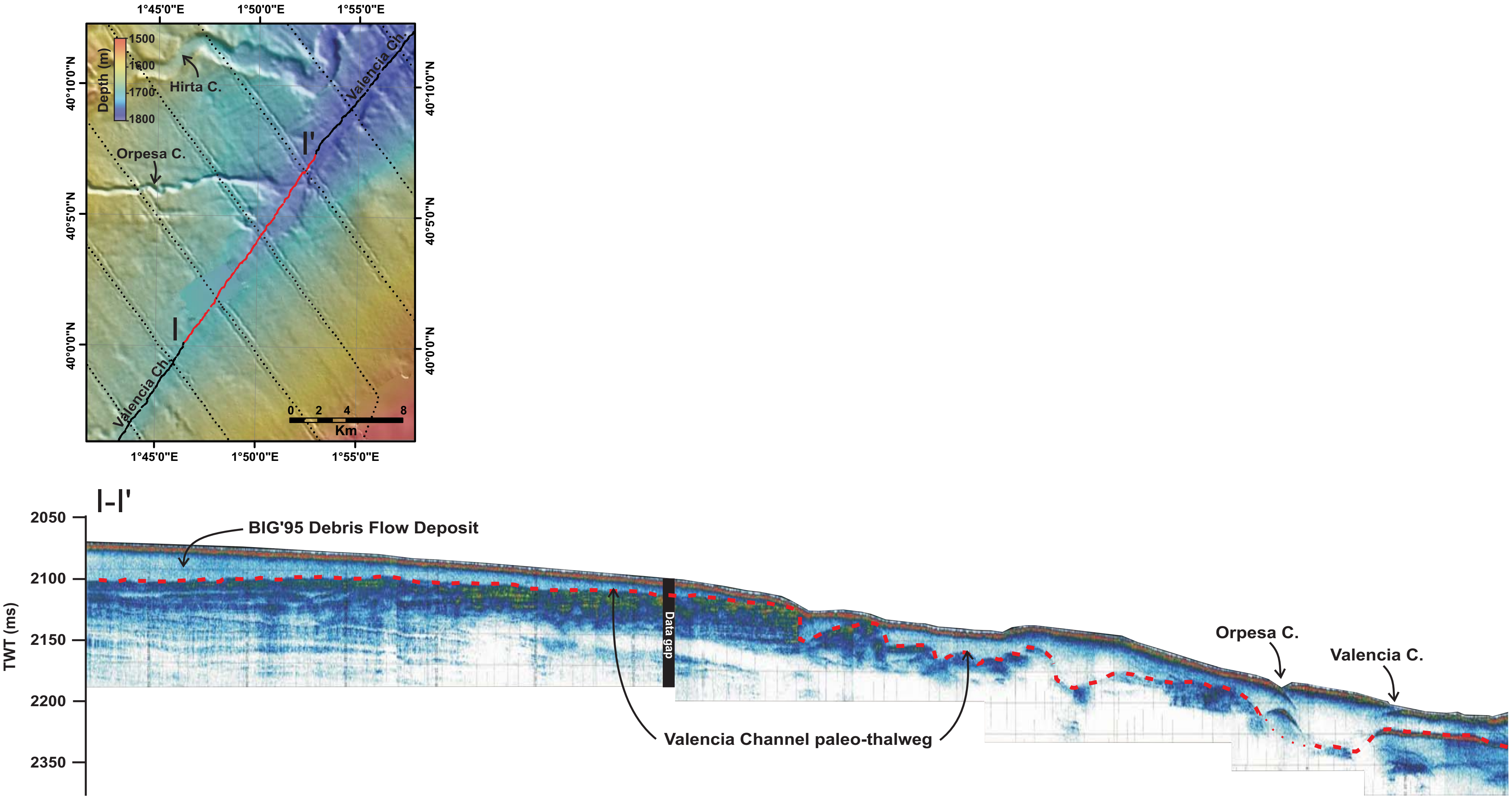

1°45'0"E
1°50'0"E
1°55'0"E
40°10'0"N
40°5'0"N
40°0'0"N
Depth (m)
1500
1600
1700
1800
Hirta C.
Orpesa C.
Valencia Ch.
I'
I
0
2
4
8
Km
I-I'
TWT (ms)
2050
2100
2150
2200
2350
BIG'95 Debris Flow Deposit
Data gap
Valencia Channel paleo-thalweg
Orpesa C.
Valencia C.

Fig.8

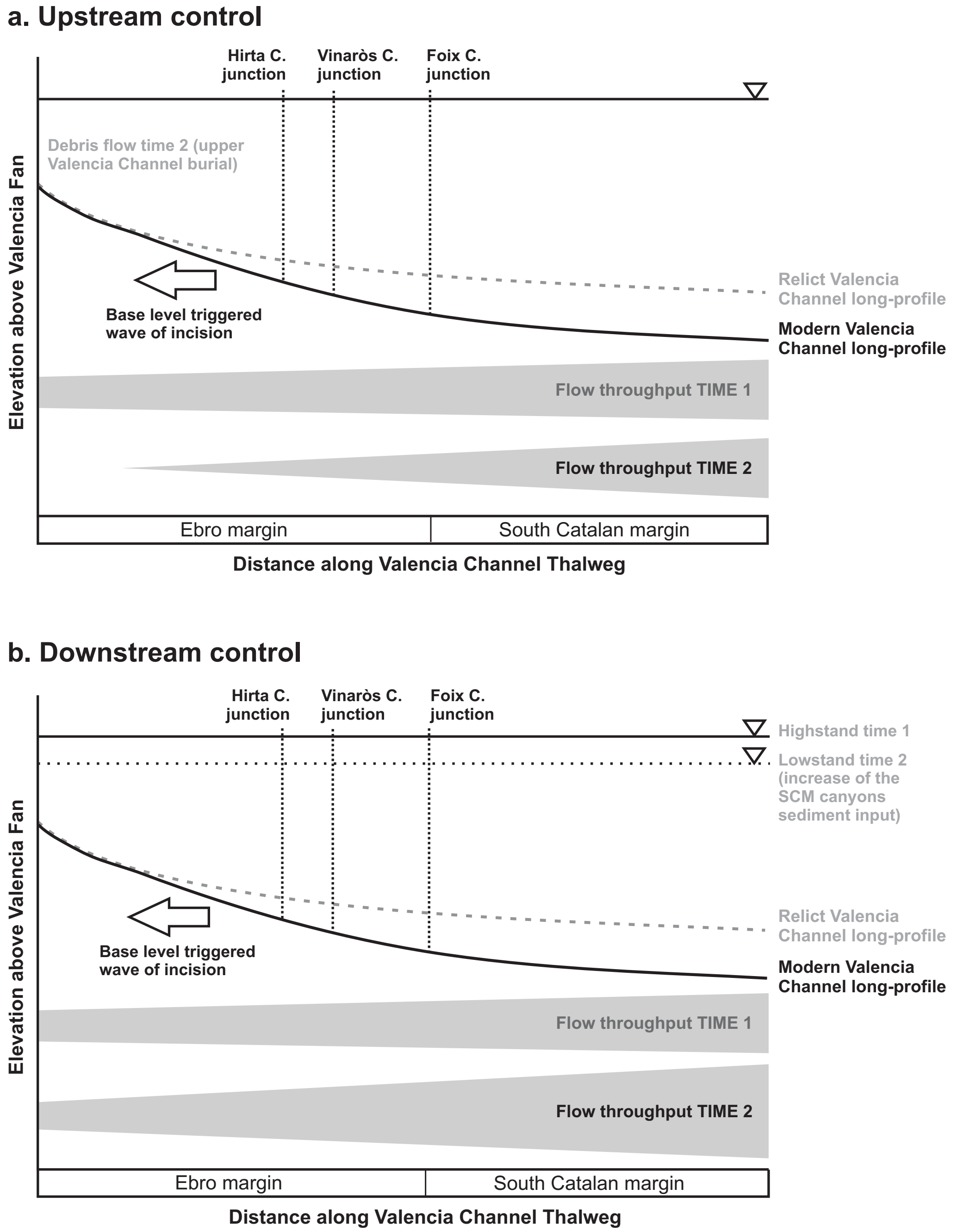
a. Upstream control
Hirta C. junction
Vinaròs C. junction
Foix C. junction
Debris flow time 2 (upper Valencia Channel burial)
Elevation above Valencia Fan
Base level triggered wave of incision
Relict Valencia Channel long-profile
Modern Valencia Channel long-profile
Flow throughput TIME 1
Flow throughput TIME 2
Ebro margin
South Catalan margin
Distance along Valencia Channel Thalweg
b. Downstream control
Hirta C. junction
Vinaròs C. junction
Foix C. junction
Highstand time 1
Lowstand time 2 (increase of the SCM canyons sediment input)
Elevation above Valencia Fan
Base level triggered wave of incision
Relict Valencia Channel long-profile
Modern Valencia Channel long-profile
Flow throughput TIME 1
Flow throughput TIME 2
Ebro margin
South Catalan margin
Distance along Valencia Channel Thalweg

Fig.9